Journal of Marine Research, 63, 1101–1125, 2005

Energetics of wind-driven barotropic variability in the Southern Ocean

by Wilbert Weijer[1,2] and Sarah T. Gille[1]

ABSTRACT

This study addresses the energetics of the Southern Ocean, in response to high-frequency wind forcing. A constant-density, multi-layer model is forced with a band of stochastically varying wind stress. The focus is on the interplay between the surface layer and the interior circulation.

In line with previous examinations, it is concluded that the interior ocean is not *directly* energized by the wind work, but rather through the work done by the pressure field. The spatial and temporal characteristics of these terms differ substantially. Although the wind work may be negative in extensive regions of the World Ocean, the pressure work energizes the interior circulation almost everywhere.

For low-frequency variability, the total work done by the wind and pressure on the barotropic flow is comparable, but discrepancies may arise for high-frequency variability. A mechanism is identified through which kinetic energy can leak from the wind-driven surface layer to the barotropic flow.

1. Introduction

The energy cycles of the ocean circulation have become a central topic in present-day oceanographic research. Knowledge of the pathways of energy through the ocean system down to the smallest, dissipative scales of turbulence is important for understanding the operation of the global overturning circulation (Munk and Wunsch, 1998; Wunsch and Ferrari, 2004). In this paper we focus on one link in the energy cycle: the transmission of wind energy from the surface layer to the ocean interior.

The energetics of the surface layer and the ocean's interior are mostly considered separately. The source term for the interior circulation is usually expressed as $s_g = \tau \cdot \mathbf{u_g}$, where τ denotes the wind stress vector and $\mathbf{u_g}$ the geostrophic velocity at the surface. The simplicity of this expression is misleading in the sense that it does not reflect the complex interplay between the Ekman flow and geostrophic motions through Ekman pumping. In fact, Fofonoff (1981) and Wang and Huang (2004a) pointed out that this wind work is actually invested in the surface flow, rather than in the ocean's interior circulation. It drives the Ekman transport up-gradient and hence tends to increase the potential energy.

1. Physical Oceanography Research Division, Scripps Institution of Oceanography, University of California, La Jolla, California, 92093-0230, U.S.A.

2. Corresponding author. ***email: wweijer@ucsd.edu***

This reservoir of potential energy can then be tapped to generate motions in the ocean's interior by means of pressure work (e.g., Gill *et al.,* 1974). Thus, although s_g provides the actual power, it is pressure work that converts this energy to a source that can drive the interior circulation.

This view points at an intimate link between the dynamics of the Ekman layer and the barotropic interior. It raises some questions about the energetics of the deep ocean. In particular, (i) what are the spatial and temporal characteristics of the pressure work in comparison to wind work, and what implications does this have for determining where the energy is dissipated? (ii) Could energy leak from the Ekman layer energy source (represented as $s_e = \tau \cdot \mathbf{u_e}$, where $\mathbf{u_e}$ is the Ekman velocity at the surface) to the interior circulation?

The Southern Ocean receives substantially more wind energy than other basins (Oort *et al.,* 1994; Wunsch, 1998; Watanabe and Hibiya, 2002; Alford, 2003; Wang and Huang, 2004a,b). A small continental area and the possibility of circumpolar circulation provide ideal conditions for intense air-sea coupling. In addition, Southern Ocean winds are exceptionally strong and extremely variable. Their spectra contain energy over a broad range of frequencies spanning low-frequency climatic fluctuations (including the Antarctic Oscillation (AAO); Thompson and Wallace, 2000), storm scales, sub-inertial, and super-inertial variability. Low-frequency variability typically contains much more energy than high-frequency fluctuations, so the spectra are essentially red. In the frequency range between 10 and 90 cycles per year (cpy), these wind stresses have spectral slopes that are estimated to be between 0.5 and 1.4, depending on the wind product (Gille, 2005). Between 100 and 363 cpy, spectral slopes are slightly steeper, between 0.7 and 2.5. In view of this uncertainty, it is important to know how sensitive the deep ocean is to the high-frequency spectral content of the wind forcing.

Although the results of Wunsch (1998) suggest that the high-frequency part of the wind forcing may not contribute substantially to the global energy budget of the interior circulation, it is generally believed that direct wind forcing is one of the main sources of eddy-kinetic energy in the ocean (Frankignoul and Müller, 1979; Müller and Frankignoul, 1981). Stammer *et al.* (2001) concluded that this mechanism is especially effective in weakly stratified areas, where the contribution of baroclinic instability mechanisms to the eddy field is small. Large *et al.* (1991) found that components of the wind (curl) forcing with frequencies up to 1/3 cpd (cycles per day) had a noticeable impact on the response of a multi-layer quasi-geostrophic model. This time scale is associated with a cut-off frequency for the excitation of Rossby waves (Willebrand *et al.,* 1980).

In this study we will address the energetics of barotropic variability of the Southern Ocean in response to high-frequency wind forcing. We will sketch the pathway of energy from the input area to the dissipative regions, distinguishing between the roles played by the Ekman and barotropic circulations. As far as we know this may be the first study to address the energetics of high-frequency wind-forced variability, explicitly discerning the roles of the Ekman layer and the interior circulation.

In the next section the model specifications will be detailed, while Section 3 will introduce the framework in which the model results will be discussed. In Section 4 the energetics of a standard run will be explored in detail, while Section 5 discusses the sensitivity of the response to the stochastic characteristics of the forcing. A discussion (Section 6) and summary and conclusion section (7) will conclude this paper.

2. The model

Our aim is to increase our qualitative understanding of energy redistributions in the Southern Ocean. Therefore, we have chosen a simplified model set-up that allows for a clear analysis of the relevant processes. The critical simplifying assumption here is the choice of wind stress forcing. Ignoring the complex wavenumber-frequency spectrum of true Southern Ocean winds, we force the model using a stochastic zonal wind stress with a fixed, large-scale spatial pattern. The amplitude is determined by a high-frequency stochastic time series with red spectrum. We will focus on high-frequency variability (frequencies larger than, roughly, 0.1 cpd). This choice allows us to consider the Southern Ocean as a constant-density, linear system, with no background circulation. The use of a simple model is justified for this paper, because the objective is to elucidate the interplay between the wind-driven layer and the ocean's barotropic interior.

For a detailed description of the model set-up we refer to Weijer and Gille (2005). The model is a constant-density version of the fully 3-D MITgcm (Marshall *et al.,* 1997a,b). This choice allows us to make a clear distinction between Ekman transports and interior barotropic flows, and is motivated by our desire to study their respective roles in the energetics of the ocean response. In shallow-water models (e.g. Hirose *et al.,* 2001) the Ekman drift and the interior circulation are merged into one single layer, blurring any distinction between the dynamics of interior and surface layer flows. This basically spreads the Ekman layer over the entire depth of the ocean, allowing it to interact with bottom topography and to affect velocity-dependent frictional closures such as bottom drag. The use of a free-surface, primitive-equations model also has advantages compared with quasi-geostrophic models (e.g. McWilliams *et al.,* 1978) which only consider balanced motions and do not account for the Ekman circulation and its energetics.

The wind forcing is applied as a body force in the upper layer of the model. Only a zonal component is used, $\tau^x(y, t_n) = \tau_0\sigma(t_n)T(y)$; here τ_0 is a basic wind stress amplitude (taken to be 0.1 N/m^2), $\sigma(t_n)$ a stochastic time series with a red spectrum, and $T(y)$ the spatial profile. T is chosen to be zonally constant, but it has a Gaussian profile in the meridional direction with a maximum at $\phi_\tau = 53$S and a 10° half-width. This profile is chosen to reflect the zonally-averaged mean zonal wind stress from climatologies (e.g., Gille, 2005).

A stochastic time series $\sigma(t_n)$ is used as described in Weijer (2005). It is constructed as a summation of N frequency components, equally distributed between f_{min} and f_{max}. The phases ϕ_i of the frequency components contain a random variable, which allows the time series to continue infinitely without repetition. The amplitudes α_i of the components are

Table 1. Experiment identifiers and spectral slopes γ of the four wind stress time series used, and their standard deviation σ.

I.D.	γ	σ
$R_{0.5}$	0.5	0.248
$R_{1.0}$	1.0	0.119
$R_{1.5}$	1.5	0.085
$R_{2.0}$	2.0	0.073

inversely proportional to the corresponding frequency through γ, which is the slope of the wind stress power spectrum. One of the advantages of this method is that it allows for restarting model runs without rendering the stochastic time series discontinuous. Only the phase of each frequency component needs to be known to continue the time series without distorting the spectral characteristics of, particularly, the low frequencies.

In this study, $N = 100$ frequency components are taken. The frequencies range from $f_{min} = 0.14$ cpd to $f_{max} = 36$ cpd, corresponding to periods between 7 days and 40 minutes (the minimum period resolved by the 20 minute time step). We present the results of 4 integrations, characterized by different values of γ. The runs will be identified as R_γ, where γ is 0.5, 1.0, 1.5 and 2.0 (Table 1). These values reflect the range of spectral slopes from different wind products (Gille, 2005). For all the experiments, the amplitude of the lowest frequency component, α_1, is kept fixed at 0.1, to account for the fact that the wind products agree reasonably well for low-frequency variability. Taken with the imposed value of γ, this determines the amplitudes of the other frequency components. This approach implies that the standard deviation σ_0 of the series depends on γ (see Table 1); the steepest spectrum with $\gamma = 2.0$ has the smallest variance and contains the least overall energy (Fig. 1).

From observations in the Drake Passage (e.g., Peterson, 1988) it is clear that the variability of the Southern Ocean is highly barotropic for sub-seasonal time scales. Koblinsky (1990) argues that the specific distribution of contours of f/H in the Southern Ocean makes it more susceptible to barotropic variability than other ocean basins. In addition, the internal Rossby radius of deformation is small in this area (about 20 km; Chelton *et al.,* 1998). A simple estimate, based on Veronis' (1956) partition equation (his Eq. 26) and Chelton *et al.*'s (1998) estimate of the Rossby radius, suggests that equipartition of energy between the baroclinic and internal modes takes place for length scales of the order of 100–200 km. For larger scales of forcing, most of the energy is absorbed by the barotropic mode. The large spatial scales and short time scales of the forcing used in this study allow us to expect a predominantly barotropic response. Note, however, that small-scale flows induced by bathymetry may violate the Rossby radius argument, and in reality may lead to some baroclinic response. But in view of the high frequencies considered here, we expect the model response to be qualitatively robust.

The small spatial scales and fast temporal scales also allow us to neglect the nonlinear metric and advective terms and to ignore any background circulation. The importance of

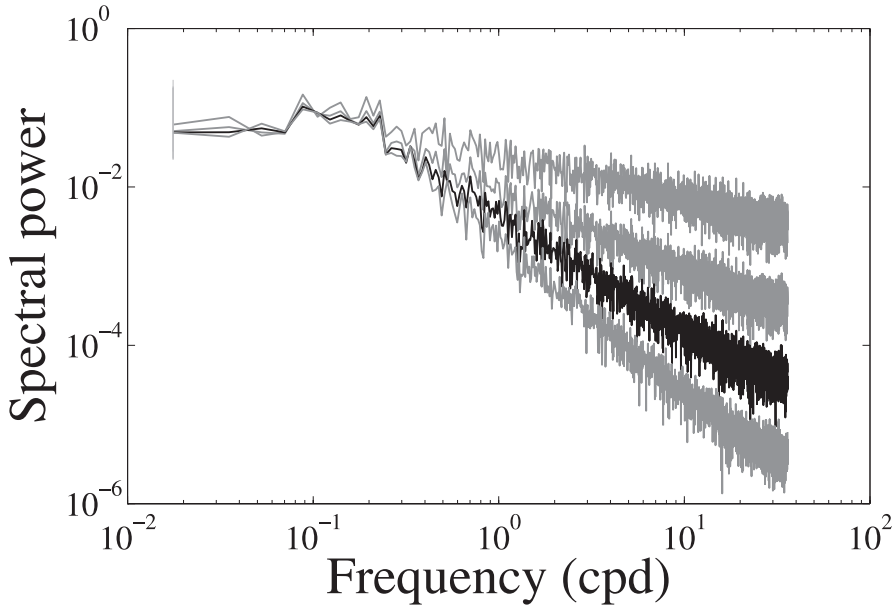

Figure 1. Spectra of the four different wind stress time series that are used. Black line denotes standard forcing time series with spectral slope $\gamma = 1.5$. Gray lines are for γ values of 0.5, 1.0 and 2.0. Error bar at the low-frequency end of the curves indicates the 95% confidence interval.

advective terms with respect to the Coriolis term is measured by the Rossby number, $\epsilon = U_0/fL$. The spatial scales of the disturbances under consideration are of the order of the external Rossby radius ($L = \mathbb{O}(2 \cdot 10^6$ m)), so a strong jet with $U_0 = 0.5$ m s^{-1} (Nowlin and Klinck, 1986) results in $\epsilon = \mathbb{O}(10^{-3})$. On time scales of roughly 5 days the advective terms are an order of magnitude smaller than the tendency term.

The model domain comprises the entire Southern Ocean, from 80S to the equator. A spherical grid is used with 180 $\times$ 80 grid points in the zonal and meridional directions, yielding a horizontal resolution of 2° $\times$ 1°. Bathymetry is based on the ETOPO-2 data set, which is interpolated onto the model grid, and smoothed with a Laplace filter. The maximum depth is set at 4000 m. The 15 grid points in the vertical are unequally distributed, with vertical grid spacing ranging from 62 m for the uppermost layer to almost 600 m for the deepest layer. The depth of the uppermost model layer is an order of magnitude larger than a characteristic e-folding depth of classical Ekman theory, so the complexities of the Ekman spiral are not nearly resolved. Instead, the surface layer in this model effectively acts as a slab-model, often used to study wind-driven inertial motions (Pollard and Millard, 1970; D'Asaro, 1985; Alford, 2003).

In Weijer and Gille (2005), the free-surface formulation of Dukowicz and Smith (1994) was used in fully implicit mode. This approach is known to damp surface gravity waves to some extent. In fact, it provided enough damping for the system to run with stress-free

boundaries so that only quadratic bottom friction was applied. In this study we are concerned with the energetics of the flow, and a semi-implicit free-surface formulation is used. This approach conserves potential energy exactly in our constant-density model. No-slip lateral boundaries are used to provide the system with a sink of energy.

Although complex algorithms have been developed to parameterize the conversion of barotropic motions to internal waves (e.g., Jayne and St. Laurent, 2001), we will adopt the conventional quadratic law to represent bottom drag, and we use a Laplacian eddy viscosity formulation for internal friction. Coefficients of horizontal and vertical eddy viscosity are $A_h = 1.0 \cdot 10^5$ m^2 s^{-1} and $A_v = 1.0 \cdot 10^{-3}$ m^2 s^{-1}, respectively. The drag coefficient for the quadratic friction law is taken to be $C_d = 0.0014$. The models are integrated for 455 days, with a time step of 20 minutes.

3. Basic energetics and sensitivity to γ

In this section we explore the sensitivity of the wind-driven energetics to the spectral slope of the forcing. First, the time-averaged balances of potential and kinetic energy will be derived, accounting for the circulation in the surface layer and the barotropic interior separately.

We start off with the barotropic, linear Navier-Stokes equations in terms of velocity $\mathbf{u} = (u, v)$ and sea surface elevation η. They represent the leading-order dynamics of the numerical model:

$$\frac{\partial \mathbf{u}}{\partial t} + f\mathbf{k} \times \mathbf{u} = -g\nabla\eta + \Gamma(z)\frac{\tau}{\rho_0 H_m} + \mathcal{F}(\mathbf{u}) \tag{1}$$

$$\eta_t = -\nabla \cdot (H\mathbf{u}). \tag{2}$$

As in the numerical model, the wind forcing τ is applied as a body forcing in the surface layer of depth H_m; the vertical structure function $\Gamma(z)$ is 1 in the surface layer and zero below. H is the total water depth, $\mathbf{k}$ is the unit vector in the vertical, and $\mathcal{F}$ denotes a friction operator, which will be left unspecified here.

The directly wind-forced motion, denoted by $\mathbf{u_s}$, is assumed homogeneous in the surface layer and hence represents an average of the Ekman drift, rather than the Ekman velocity at the surface of the ocean. Underneath this surface layer, the flow is to a large extent depth-independent and pressure-driven; for our choice of frictional parameters horizontal viscosity is the dominant frictional process, so deviations in the bottom boundary layer are small. This allows us to express the velocity field in terms of $\mathbf{u_s}$ and a homogeneous interior contribution $\mathbf{u_b}$ as: $\mathbf{u}(x, y, z) = \mathbf{u_b}(x, y) + \Gamma(z)\mathbf{u_s}(x, y)$. The (linear) momentum equations Eq. (1) can now be decomposed to describe the wind- and pressure-driven flow components:

$$\frac{\partial \mathbf{u_s}}{\partial t} + f\mathbf{k} \times \mathbf{u_s} = \frac{\tau}{\rho_0 H_m} + \mathcal{F}(\mathbf{u_s}) \tag{3}$$

$$\frac{\partial \mathbf{u_b}}{\partial t} + f\mathbf{k} \times \mathbf{u_b} = -g\nabla\eta + \mathcal{F}(\mathbf{u_b}), \tag{4}$$

where it is understood that Eq. (3) is only defined for the surface layer.

Vertically-integrated kinetic energy, defined as $E = \frac{1}{2}\rho_0 \int_{-H}^{0} \mathbf{u} \cdot \mathbf{u} dz$, can be decomposed accordingly into a barotropic part, a surface layer component and a mixed contribution:

$$E_s = \frac{1}{2}\rho_0 H_m(\mathbf{u_s} \cdot \mathbf{u_s}) \tag{5a}$$

$$E_b = \frac{1}{2}\rho_0 H(\mathbf{u_b} \cdot \mathbf{u_b}) \tag{5b}$$

$$E_{bs} = \rho_0 H_m(\mathbf{u_b} \cdot \mathbf{u_s}). \tag{5c}$$

Their time-rate of change can be derived by multiplying Eq. (3) by $\mathbf{u_s}$, Eq. (4) by $\mathbf{u_b}$, and taking the sum of $\mathbf{u_b}$ times Eq. (3) and $\mathbf{u_s}$ times Eq. (4):

$$\frac{\partial E_s}{\partial t} = s_s + d_s \tag{6a}$$

$$\frac{\partial E_b}{\partial t} = p_b + d_b \tag{6b}$$

$$\frac{\partial E_{bs}}{\partial t} = p_s + s_b + d_{bs}. \tag{6c}$$

where:

$$p_s = -\rho_0 g H_m \mathbf{u_s} \cdot \nabla\eta \tag{7a}$$

$$p_b = -\rho_0 g H \mathbf{u_b} \cdot \nabla\eta \tag{7b}$$

$$s_s = \mathbf{u_s} \cdot \tau \tag{7c}$$

$$s_b = \mathbf{u_b} \cdot \tau \tag{7d}$$

$$d_s = \rho_0 H_m \mathbf{u_s} \cdot \mathcal{F}(\mathbf{u_s}) \tag{7e}$$

$$d_b = \rho_0 H \mathbf{u_b} \cdot \mathcal{F}(\mathbf{u_b}) \tag{7f}$$

$$d_{bs} = \rho_0 H_m[\mathbf{u_b} \cdot \mathcal{F}(\mathbf{u_s}) + \mathbf{u_s} \cdot \mathcal{F}(\mathbf{u_b})]. \tag{7g}$$

In our stochastically forced model we are interested in the time-averaged energetics, which can be written as a double time-integral of the source and sink terms:

$$\langle E_s \rangle = \langle S_s \rangle + \langle D_s \rangle \tag{8a}$$

$$\langle E_b \rangle = \langle P_b \rangle + \langle D_b \rangle \tag{8b}$$

$$\langle E_{bs} \rangle = \langle P_s \rangle + \langle S_b \rangle + \langle D_{bs} \rangle \tag{8c}$$

where $\langle \cdot \rangle = (1/\Pi) \int_0^\Pi \cdot \, dt$, Π being the period of integration, and $P_b = \int_0^t p_b dt'$, etc. In the rest of this manuscript the brackets will be dropped for convenience, but time-averaged values are still implied unless otherwise noted. The terms p, s and d denote the rate of work by pressure forces, wind stress and friction, respectively. Their capital letter counterparts denote the average of the total energy exchanged by the corresponding terms since the start of the integration.

Potential energy is defined as $U = \frac{1}{2}\rho_0 g(\eta^2 - H^2)$, and its time-derivative is given by:

$$\frac{\partial U}{\partial t} = m_b + m_s, \tag{9}$$

where:

$$m_b = -\rho_0 g \eta \nabla \cdot (H \mathbf{u_b}) \tag{10a}$$

$$m_s = -\rho_0 g \eta \nabla \cdot (H_m \mathbf{u_s}). \tag{10b}$$

As before, we will consider time-averaged quantities:

$$\langle U \rangle = \langle M_b \rangle + \langle M_s \rangle. \tag{11}$$

Again, the capitals denote the average of the total energy exchanged by the corresponding term, and the brackets will be dropped in the following.

Comparing the pressure work terms p and the divergence terms m, we see that they are both components of the divergence of the energy fluxes $\mathbf{g_b} = \rho_0 g \eta H \mathbf{u_b}$ and $\mathbf{g_s} = \rho_0 g \eta H_m \mathbf{u_s}$. In fact, the spatial integrals of $\nabla \cdot \mathbf{g_b}$ and $\nabla \cdot \mathbf{g_s}$ are zero due to the no-normal flow condition on the boundaries. This means that the spatial integrals of m_b and p_b, and of m_s and p_s, add up to zero. Note that:

$$p = -\nabla \cdot \mathbf{g} - m. \tag{12}$$

Figure 2a shows the input of kinetic energy by the wind stress as a function of the spectral power of the forcing. The energy input in the Ekman layer (S_s) is strongly affected by the spectral characteristics of the forcing. A factor of 40 difference is achieved between $R_{0.5}$ and $R_{2.0}$. In addition, there is a strong, factor 20 change in kinetic energy of the Ekman drift itself (E_s in Fig. 2b).

This contrasts with the wind work on the interior flow (S_b) and the kinetic energy of the interior flow (E_b). S_b is basically insensitive to the value of γ, but E_b decreases by a factor of 2.4 as γ increases. One may then wonder how the interior flow is energized. In the next sections we will look at the balances and redistributions of energy, first for the standard run $R_{1.5}$, and then for cases with other values of γ.

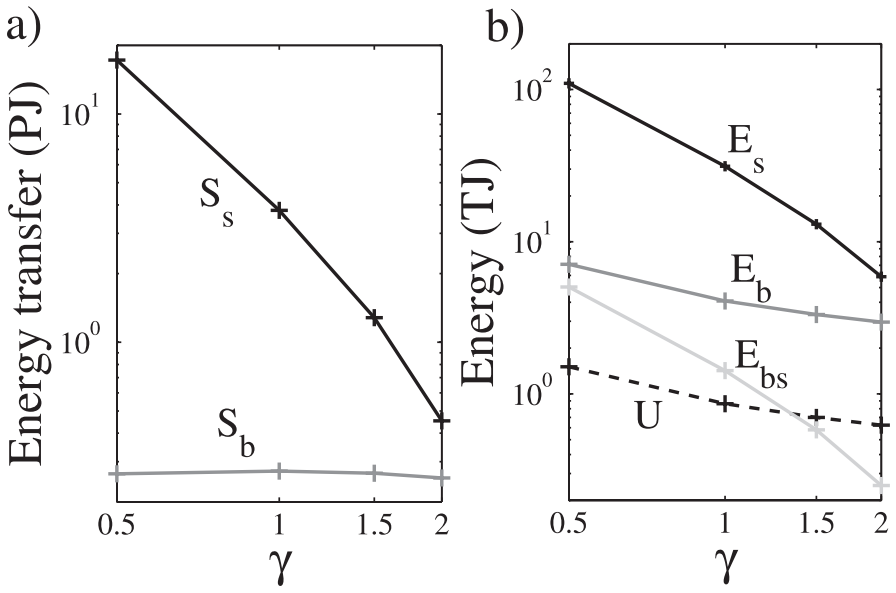

Figure 2. (a) Kinetic energy input and (b) energy content as a function of spectral slope γ of the forcing time series. Source terms are plotted for the Ekman (black line) and barotropic (gray) modes, and are surface-integrated. They represent the terms as they appear in the balance of time-averaged kinetic energy, and hence are a double integral over time (Eq. (8)). Energy contents represent time-averaged kinetic energy of the surface layer (E_s, black), barotropic (E_b, dark gray) and mixed ($-E_{bs}$, light gray) modes, as well as potential energy (U, black dashed). Note that E_{bs} is negative.

4. Energetics of $R_{1.5}$

a. Time-averaged distributions of energy

Figure 3 shows the time-averaged fields of kinetic energy and its components E_s, E_b, and E_{bs}. The distribution of kinetic energy is concentrated in the forcing region. The surface flow contribution E_s is distributed homogeneously in a broad band, which is obstructed only by the tip of South America. The kinetic energy of the abyssal flow, on the other hand, is much more patchy. The highest values of E_b are found where the flow has to squeeze through gaps in between bathymetric features. In contrast to the quadratic quantities E_s and E_b, the mixed-mode kinetic energy E_{bs} has no definite sign. Yet, Fig. 3d shows that it is negative almost anywhere. According to its definition Eq. (5c), this reflects the fact that the interior and surface circulations consistently flow in the opposite direction, with the barotropic flow compensating for the Ekman transport. E_{bs} shows up as a broad and weak band in the forcing area, and has a few isolated maxima above the Kerguelen Plateau, the Macquarie Ridge, and around the tip of South America.

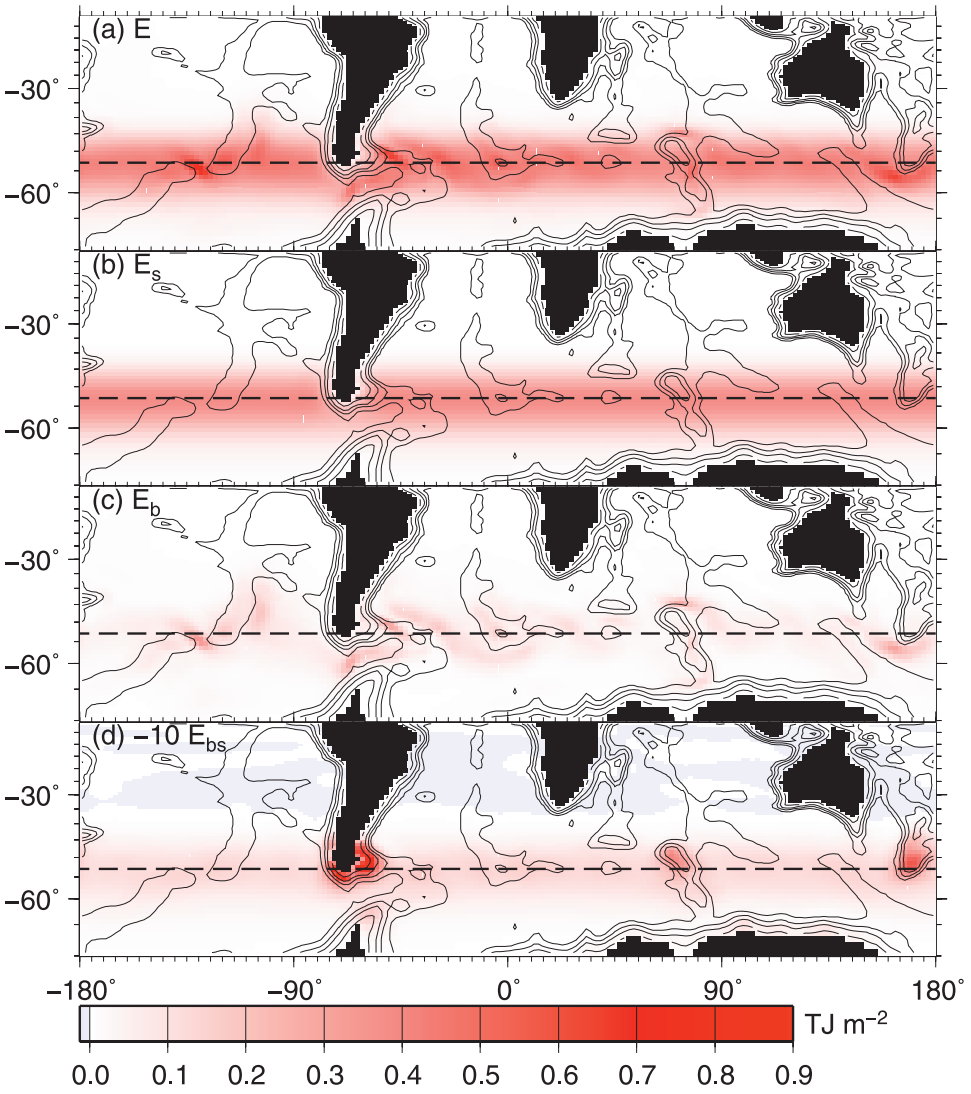

Figure 3. Time-averaged fields of (a) kinetic energy E and its constituents (b) E_s, (c) E_b, and (d) $-10E_{bs}$. Black dashed line denotes axis of maximum wind stress forcing, thin black lines are 500, 1500, 2500 and 3500 m isobaths.

b. Energy balances

Figure 4a shows the zonally-averaged terms in the (time-averaged) kinetic energy balance, Eqs. (8). These terms add up to the zonally-averaged kinetic energy, which would be indistinguishable from zero in this plot. The dominant terms reflect the energetics of the Ekman balance, in which the kinetic energy input by the wind stress (S_s) is locally

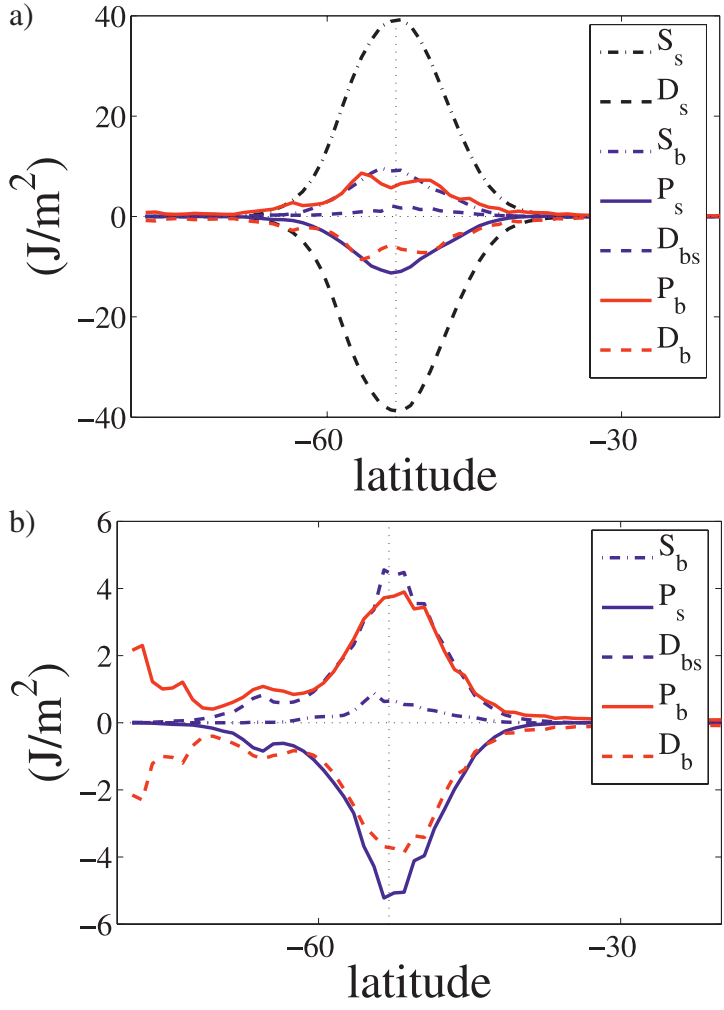

Figure 4. (a) Zonally averaged source and sink terms of the time-averaged kinetic energy. Shown are the contributions by the wind stress (S, dash-dotted lines), viscous dissipation (D, dashed), and pressure work (P, solid) to the surface (black), mixed (blue) and barotropic mode (red) kinetic energies, as in Eqs. (8). Vertical dotted line denotes the latitude of maximum wind stress at 53S. (b) As Figure 4, but now for the differences $R_{1.0} - R_{2.0}$. Only the terms contributing to E_{bs} and E_b are plotted.

dissipated in the mixed layer by turbulent processes (D_s); the remaining terms are basically of the same order of magnitude and will be discussed in the following paragraphs.

i. Wind stress and pressure work done on the interior flow. As observed by Fofonoff (1981) and Wang and Huang (2004a), the energy input by the wind stress into geostrophic

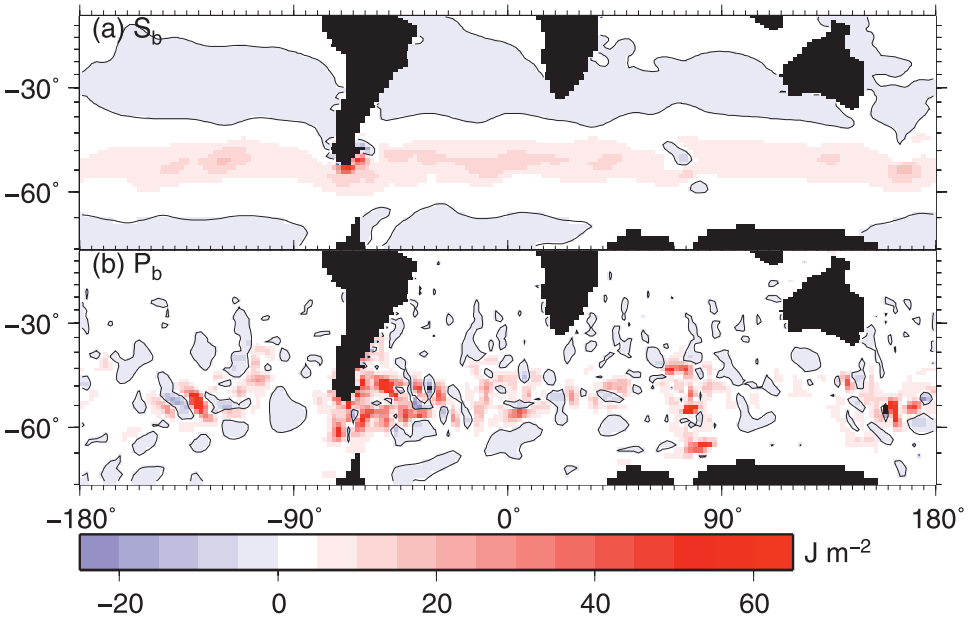

Figure 5. (a) Source term S_b and (b) pressure work term P_b. Black lines are the zero-contours.

flow is mostly used to push the Ekman transport up-pressure. This can be seen by rewriting the pressure work term p_s as:

$$p_s = -\rho_0 g H_m v_s \eta_y = -\rho_0 g \left(\frac{-\tau^x}{\rho_0 f}\right)\left(\frac{-f u_g}{g}\right) = -\tau u_g, \tag{13}$$

where u_g denotes the zonal geostrophically balanced surface velocity. Indeed, Figure 4a shows that the wind work S_b and pressure work P_s nearly cancel. The difference is accounted for by a friction term D_{bs}, which will later be shown to play an important role for smaller values of γ.

If we neglect this frictional coupling between the surface circulation and the interior, it is the pressure work P_b that actually drives the interior circulation, rather than the wind work S_b. This allows the system to release the energy at places where it may be more efficiently dissipated. Figure 5 shows that S_b has a mainly zonal structure, with highest values in the region of maximum wind stress forcing. In addition, there are large areas (mainly in the mid-latitude basins) where wind stress extracts energy from the flow. The term P_b, however, is much more patchy, and more consistently positive throughout the entire domain; it shows strong correlations with topographic features, and, naturally through Eq. (8b), with the dissipation term D_b. In the areas where P_b is negative, viscous friction locally energizes the flow ($D_b > 0$) as it extracts momentum from its surroundings.

There is also a spectral difference between the work terms S_b and P_b. Figure 6 shows that the spectrum of E_b (no time-averaging implied) contains substantial amounts of

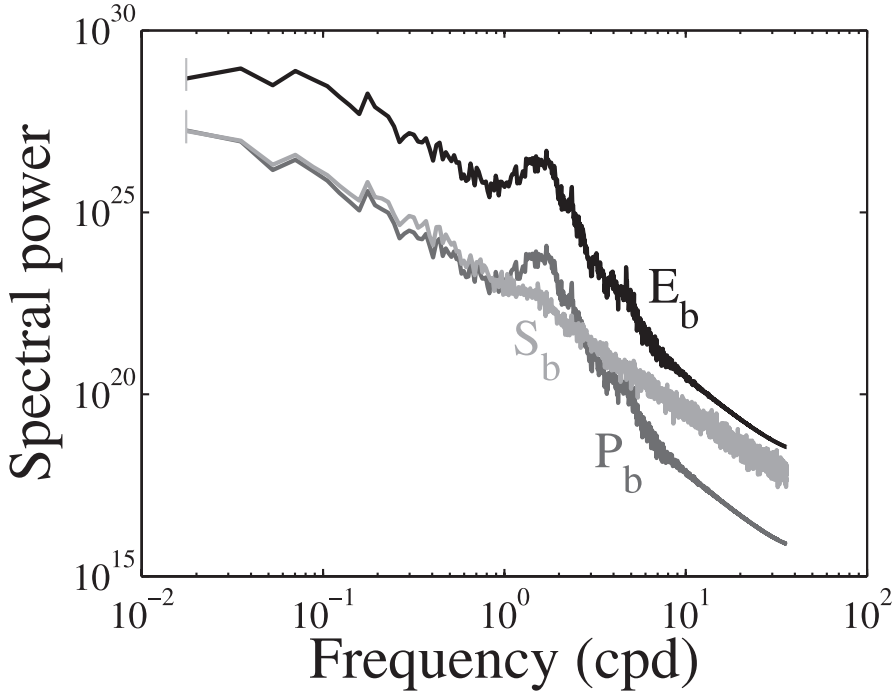

Figure 6. Spectra of the time series of globally-integrated kinetic energy of the barotropic flow E_b, and of the source terms S_b and P_b (no time-averaging is implied here). Spectra are an average of 8 subsamples of the time series, light-gray bars denote 95% confidence level. Time series are detrended and prewhitened. The spectrum of E_b is offset by a factor of 400 for clarity.

inertial energy. The spectrum of S_b (no time-averaging), on the other hand, only shows minor elevations in the inertial band; the variability in energy input it reflects is obviously not enough to explain the enhanced levels of global kinetic energy. In contrast, the spectral content of P_b (no time-averaging) is basically identical to that of E_b.

S_b may be an actual source of kinetic energy for the ocean circulation, but it cannot be considered as the primary source of energy for the interior flow; additional conversions involving the Ekman layer take place to transfer energy to the interior flow. The actual source of energy is the work done by pressure, and we have shown that both the spatial and the temporal characteristics of P_b and S_b differ. How this energy transfer takes place will be studied in the next paragraph.

ii. Energetic coupling of surface and interior flows. The following thought experiment may serve to illustrate the role of the Ekman circulation in the energetics of the wind-driven motions. Consider a situation in which the sea surface can be deformed by divergences in the Ekman transports (V_s) only, hence allowing for large-amplitude deviations (η_s) that are not affected by compensating motions in the ocean's interior.

Given our idealized wind stress profile T, this would lead to an energy flux $g_{s,s} = \rho_0 g \eta_s V_s \propto -[(T/f)^2]_y$ (Eq. A3; see the Appendix for details). This flux transports energy away from the axis of maximum wind stress (Fig. 10) to the latitude bands around 60S and 46S, where Ekman pumping is strongest. Here it is stored as potential energy via a contribution to M_s: $M_{s,s} = -\rho_0 g \eta_s V_{s,y} \propto [(T/f)_y]^2$ (Eq. A5). The energy is extracted from the Ekman flow, which has to do work against a gradient in sea-level η_s: $P_{s,s} = -\rho_0 g V_s \eta_{s,y} \propto T/f(T/f)_{yy}$ (Eq. A6). At the central axis of the wind stress profile the strongest Ekman transport flows against the largest gradient in η_s. The dotted lines in Figure 7 show these terms, attenuated by a factor of 10. Clearly, the work and divergence terms of the Ekman component (P_s and M_s) reflect in shape and sign the terms $P_{s,s}$ and $M_{s,s}$.

The interior motion largely compensates for the sea-level deformations induced by the Ekman transport, and accounts for a sea-level deviation that we could indicate by η_b (so that $\eta = \eta_s + \eta_b$). This compensation reduces the work that has to be done by the Ekman transport (via a term that we could denote by $P_{s,b} = -\rho_0 g V_s \eta_{b,y}$), and the amount of potential energy that can be stored (by an amount equal to $M_{s,b} = -\rho_0 g \eta_b V_{s,y}$). More importantly, the pressure field can tap the stored potential energy (M_b) and convert it to kinetic energy of the interior flow (P_b). Only a small residual of potential energy M remains unused (Fig. 7b), since the ocean only allows for small deviations of the sea surface. This means that almost the entire supply of potential energy M_s is immediately used by the interior flow.

Not all of the energy available to the interior flow returns to the central axis of forcing to compensate for P_s. Hence, net energy is extracted from the total flow in the central band of wind stress forcing (Fig. 7a, negative P between 60S and 46S), while energy is re-invested outside this band. Figure 7c shows the zonal integral of these meridional fluxes G.

5. Energetics: sensitivity to spectral slope

In the previous section we described the balances and redistributions of energy for the standard run. Here we will consider the differences between the runs with different spectral slopes γ. To find out how an increase in interior kinetic energy E_b can be accounted for when the wind work S_b does not change, we will compare the energetics of the runs $R_{1.0}$ and $R_{2.0}$ to see how the flows of energy change when more energy is available at high frequencies.

Figure 4b shows how the terms pertaining to the balances of E_{bs} and E_b change when γ is decreased from 2.0 to 1.0. This change flattens the spectrum and increases the energy at high frequencies. It confirms that the wind work on the barotropic mode (S_b) hardly changes. Nevertheless, the pressure work (P_b) is considerably enhanced, as is the associated dissipation D_b. This is consistent with the increase in kinetic energy of the interior flow, E_b (Fig. 2).

Where does this extra energy come from? For the standard run, this energy P_b is largely balanced by the work done against the pressure field by the surface flow, P_s, for which, in turn, energy is supplied by the wind stress through S_b. Figure 4b shows the corresponding

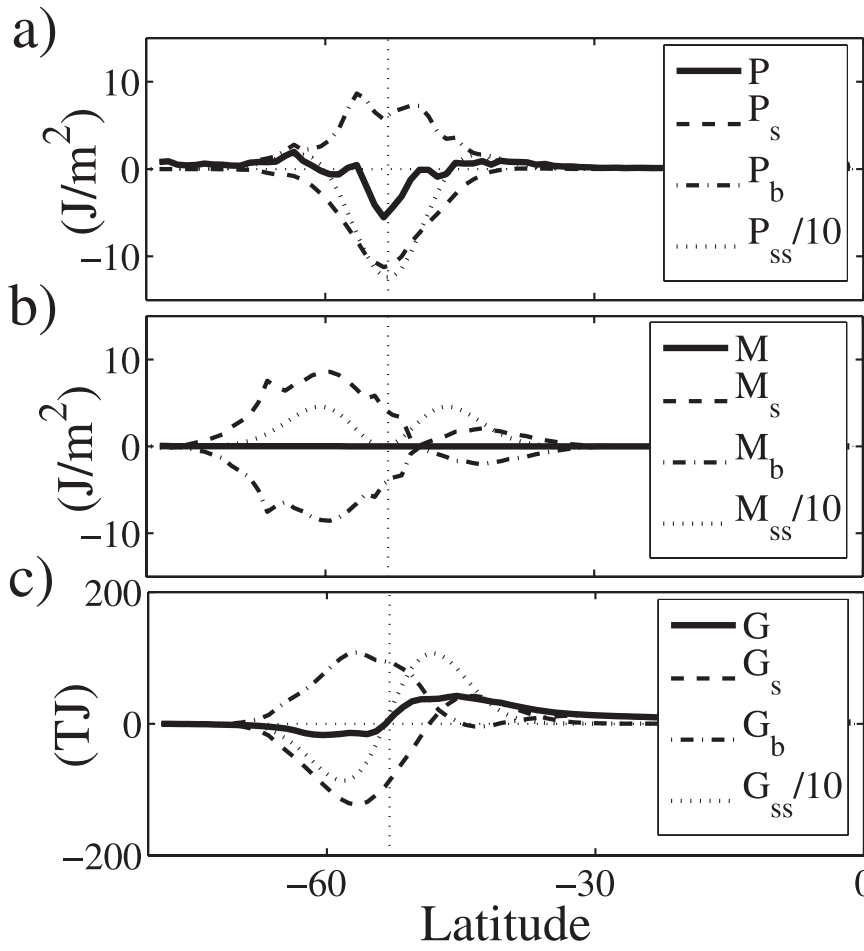

Figure 7. (a) Zonally-averaged pressure work P and (b) divergence contribution to the potential energy equation M, and (c) zonally integrated meridional flux of energy G. Contributions of surface layer (dashed) and barotropic interior (dash-dotted) add up to total (solid). Dotted lines denote the $P_{s,s}$, $M_{s,s}$ and $G_{s,s}$ terms (attenuated by a factor of 10) which would reflect P_s, M_s and G_s if divergences of the Ekman transport were the only factors able to deform the surface. See text for explanation.

increase in P_s, but it is obviously not balanced by an increase in S_b. Instead, it is drawn from the wind work on the surface layer, S_s. The term that is responsible is the viscous coupling between the Ekman and barotropic modes, D_{bs} (Fig. 8).

The mixed mode kinetic energy E_{bs} is a correction term: when $\mathbf{u_s}$ and $\mathbf{u_b}$ are in the same direction, the sum of the barotropic and kinetic energies E_b and E_s underestimates the total kinetic energy, and the correction term E_{bs} is positive. In our model, E_{bs} is largely negative (Fig. 3d), suggesting that $\mathbf{u_s}$ and $\mathbf{u_b}$ are in opposite direction; in this case they partly cancel

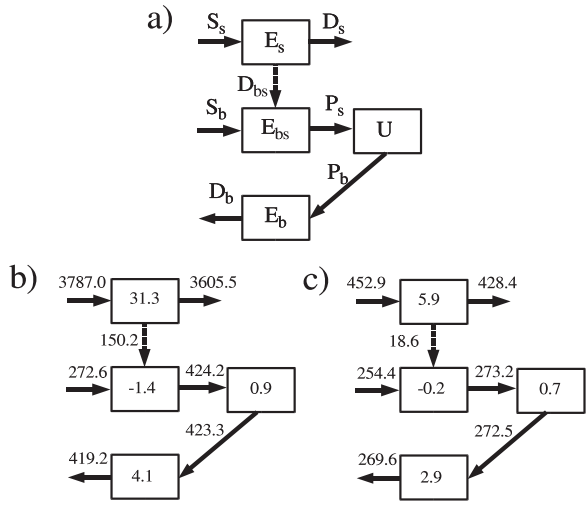

Figure 8. (a) Diagram of the time-mean, volume-integrated energies and energy flows as in Eqs. (8), and their numerical values for (b) $R_{1.0}$ and (c) $R_{2.0}$.

and $E_b + E_s$ overestimates the kinetic energy. Indeed, coherence analysis shows that the wind- and pressure-driven transport components are consistently 180° out of phase throughout the frequency spectrum.

Just as the dissipation terms D_b and D_s tend to reduce the kinetic energies E_b and E_s, D_{bs} tends to reduce the magnitude of E_{bs}, so they are of opposite sign in Eq. (8c). This means that it cannot be interpreted as a transfer of energy from the Ekman mode to the barotropic mode: D_{bs} just dissipates kinetic energy of the Ekman mode due to friction with the barotropic mode, and vice versa (see Eq. (7g)).

The significance of this term may be illustrated by the example shown in Figure 9: suppose that the surface layer is forced by a constant westerly wind, τ. Assuming for simplicity that the flow is damped by Rayleigh friction, so that $\mathcal{F}(\mathbf{u}) = -r\mathbf{u}$, the slab model of the surface layer predicts a steady Ekman flow with components:

$$\mathbf{u_s} = (u_s, v_s) = (r, -f)\,\frac{\tau}{\rho_0 H_m (r^2 + f^2)} \tag{14}$$

Note that the two velocity components are related through: $u_s = -rv_s/f$. Suppose further that a barotropic flow balances the Ekman transport exactly:

$$\mathbf{u_b} = (u_b, v_b) = (-\delta u_s, -\delta v_s). \tag{15}$$

Here, $\delta = H_m/H$, is the fractional depth of the surface layer. This flow is associated with a zonal tilt in sea-level:

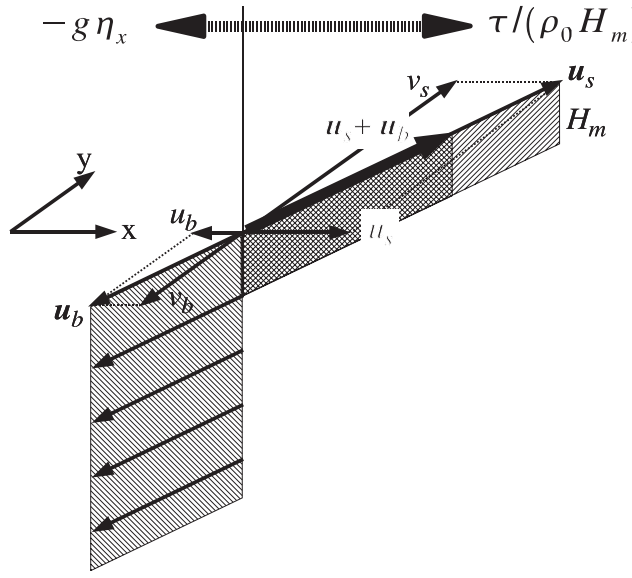

Figure 9. Set-up of example problem, as discussed in the text. The surface layer of depth H_m is forced by a constant, zonal wind stress τ, which forces an Ekman transport $\mathbf{u_s} = (u_s, v_s)$ in the upper layer. This transport is compensated by a barotropic interior flow $\mathbf{u_b} = (u_b, v_b) = (-\delta u_s, -\delta v_s)$, where $\delta = H_m/H$. This flow is driven by a tilt in the sea-level η. The actual surface layer velocity is now $\mathbf{u_s} + \mathbf{u_b} = (1 - \delta)\mathbf{u_s}$.

$$g\eta_x = \frac{r^2 + f^2}{f} v_b = \delta \frac{\tau}{\rho_0 H_m}. \tag{16}$$

In this context, the balances of energy as given by Eq. (6) can be expressed as:

$$\frac{\partial E_s}{\partial t} = s_s + d_s = \alpha - \alpha = 0 \tag{17a}$$

$$\frac{\partial E_b}{\partial t} = p_b + d_b = \delta\alpha - \delta\alpha = 0 \tag{17b}$$

$$\frac{\partial E_{bs}}{\partial t} = p_s + s_b + d_{bs} = -\delta\alpha - \delta\alpha + 2\delta\alpha = 0. \tag{17c}$$

where:

$$\alpha = \frac{r\tau^2}{\rho_0 H_m (r^2 + f^2)}. \tag{18}$$

The total dissipation in the surface layer can be written as $d_s + d_{bs} + \delta d_b$, where the last contribution is the fraction of the dissipation of the barotropic flow that takes place in the

surface layer. This sum equals $-(1 - \delta)^2\alpha$, which is a fraction $(1 - \delta)$ smaller than the reduction in the energy input by the wind, $s_s + s_b = (1 - \delta)\alpha$.

This example illustrates how the presence of a significant barotropic flow component in the surface layer affects the source and sink terms of the energy balance differently: when the surface and interior flows are in opposite direction, the dissipation is reduced more than the work done by wind stress. This leaves a residual of energy that can be used by the Ekman flow to perform work against the pressure field (and in this case also by the barotropic flow to perform work against the wind: $s_b < 0$). In this way, extra energy is supplied to the ocean's interior, without increasing the wind work performed on the barotropic flow (which is negative in this example).

In the latitude band of the Drake Passage no net zonal pressure gradient can be sustained, so this example might appear only to be applicable to the area north of the Drake Passage. In the unbounded latitudes, one would expect a flow that is locally controlled by friction, and a barotropic circulation that is *perpendicular* to the surface flow. However, Weijer and Gille (2005) have shown that the flow in the Southern Ocean interacts strongly with bathymetry, and that topographic form stress plays an important role in the momentum balance. Hence, pressure gradients can be sustained locally between bathymetric features, explaining the fact that even in the unbounded region $\mathbf{u_s}$ and $\mathbf{u_b}$ are close to 180°, rather than 90°, out of phase.

6. Discussion

The ocean's response to external forcing is constrained by several balances, each governing a different aspect of the flow. The energy balance imposes fewer constraints on the ocean circulation than do the balances of vorticity and momentum. In other words, many different flow configurations can satisfy the energy balance, while fewer configurations are consistent with the vorticity or momentum balances. This is nicely illustrated by some additional numerical experiments in which the frictional parameters were varied: neither vertical friction nor bottom friction contributes significantly to the kinetic energy balance, and reducing the coefficient of horizontal friction only slightly alters the terms in the energy balance. The reason is that the topographic form stress is the dominant retarding mechanism in the momentum balance, as shown by Weijer and Gille (2005). But interestingly, this mechanism does not appear explicitly in the balance of kinetic energy (MacCready *et al.,* 2001). A change in, for instance, the horizontal friction parameter A_h changes the field of kinetic energy to some extent, but this seems to be intended solely to maintain the energy sink that is required by other processes.

Whether or not the wind work s_b *directly* forces the interior circulation is still a matter of some confusion in present-day literature (e.g., Scott, 1999; Wunsch and Ferrari, 2004). Although s_b provides the actual power, it is pressure work p_b that truly delivers this energy at depth (e.g., Gill *et al.,* 1974). This may clear up a few ambiguities. The first is the principle that purely geostrophic flow is essentially balanced, and to leading order non-dissipative (Pedlosky, 1987). If the subsurface geostrophic flow were to receive

energy through wind work it would also require a way to dissipate, which is at odds with the conservative nature of purely geostrophic flows.

Secondly, there are extensive regions in the World Ocean where wind work is negative (Wunsch, 1998). At first sight, this may seem remarkable, since the balance of kinetic energy must be closed locally wherever nonlinear advection terms are negligible. And in the ubiquitous presence of friction, there would be no source of energy to keep the water in motion. However, we have shown that the spatial distribution of pressure work differs substantially from the wind work. The pressure work is mainly positive throughout the entire ocean, so that even in the areas where wind work is negative the pressure field can maintain flow against friction. In addition, the spectrum of P_b closely matches the spectrum of E_b, with enhanced levels of energy in the inertial band. The spectrum of S_b, on the other hand, is basically straight, and unable to explain the spectrum of E_b. The difference is especially pronounced for very high frequencies in the inertial range.

Thirdly, the barotropic mode may be able to extract kinetic energy from the Ekman mode. The sensitivity studies show that a flatter forcing spectrum (smaller γ) does not change the wind work term S_b, but increases the level of kinetic energy in the interior substantially. Coupling between the interior flow and the Ekman transport (D_{bs}) reduces the net dissipation in the Ekman layer, yielding a surplus of energy that can be used to enhance P_s, and thereby P_b. The insensitivity of this process with respect to the friction parameter A_h suggests that it is rather robust, and hence may be a consistent feature in systems where the barotropic velocity is a significant fraction of the Ekman flow.

The presence of (near-)inertial energy in the interior ocean is usually ascribed to internal waves propagating downward from the mixed layer, or upward from the bottom (e.g., Garrett and Munk, 1979; Fu, 1981). Hypotheses involving loss of balance, and the resulting excitation of inertial waves (the Rossby adjustment problem; e.g., Veronis, 1956; Gill, 1982) are not generally put forward. Veronis and Stommel (1956) already concluded that in their two-layer model, baroclinic inertial oscillations were much stronger than their barotropic counterparts. Although there are some indications that moving storms may excite depth-independent inertial motions (Shay *et al.,* 1990), it seems that the length scales of synoptic variability in the atmosphere facilitate the excitation of baroclinic inertial motions instead (Ginis and Sutyrin, 1995). It is therefore likely that the large spatial scale of our forcing, and its static character, may have facilitated the excitation of barotropic inertial motions in this model.

Baroclinicity may complicate the simple picture sketched in this paper in several other ways. In a stratified ocean, the work term p_s can additionally store potential energy by deflecting isopycnals (Gill *et al.,* 1974). Energy stored in this form (often expressed in terms of Available Potential Energy; Huang, 1998) can be tapped by baroclinic motions. This effect is significant when substantial Ekman pumping velocities are achieved, i.e., for steady or slowly-varying winds with relatively small spatial scales. The high frequencies and large spatial scale of the forcing used in this study hence seem to warrant the barotropic approach.

However, a substantial amount of barotropic energy may be lost to the internal mode when the flow interacts with topography (e.g., Holland, 1975; Ivchenko *et al.,* 1997; Simmons *et al.,* 2004; Arbic *et al.,* 2004). Steady and transient flows over topography may generate internal waves that provide a drag on the barotropic flow (Bell, 1975). There are basically two regimes: the regime of oscillatory flow, and that of (almost) steady flow over varying bottom topography. Simmons *et al.* (2004) estimate that in their global 10-layer tide model, forced by an M_2 tidal frequency only, 30% of the barotropic tidal energy was converted to the internal mode. However, oscillatory flow can only excite internal mode gravity waves for frequencies above the local inertial frequency. At 53°, the latitude where in our model the wind forcing is strongest, this period is 15 hr, and hence the absence of baroclinicity in our model is likely to underestimate the damping in the super-inertial regime. The wind stress forcing applied to our model only contains a small fraction of energy in the super-inertial band, so baroclinic conversion is probably less important than in tide models (e.g., Arbic *et al.,* 2004).

When the flow U is almost steady but the topography is bumpy, the frequency with which the flow encounters ridge crests is given by Uk, where k^{-1} is a characteristic length scale of the topography (Gill, 1982). Again, only when this frequency exceeds the local inertial frequency is the generation of internal waves possible. A characteristic velocity scale of $U = 0.01$ m s^{-1}, and a minimum resolved topographic wavelength $\lambda = 2\Delta x \sim 2 \cdot 10^5$ m, yield an upper bound to the encounter frequency of $3.1 \cdot 10^{-7}$ s^{-1}. Hence it seems unlikely that the inclusion of stratification in our model would have generated a substantial baroclinic response.

Mesoscale eddies play an important role in the energetics of the Southern Ocean. Ivchenko *et al.* (1997) studied the energetics of the Southern Ocean in the high-resolution model FRAM, and found that, as in our model, the dominant sink of eddy kinetic energy (EKE) was lateral friction. The main sources of EKE were found to be transfer from eddy potential energy (resulting from baroclinic instability processes) and non-linear transfer from the mean circulation (barotropic instability). They ascribe the lack of wind-induced eddy-variability to the wind stress forcing of the model, which is by climatological (monthly mean) winds. The schematic wind stress in our model does not allow us to estimate this term from our results.

7. Summary and conclusion

In this paper we addressed the energetics of the Southern Ocean in response to high-frequency wind stress variability. The main issue at hand was the interaction between the Ekman flow and the ocean's interior (barotropic) circulation. The source of energy for the interior flow is often expressed as $s_g = \boldsymbol{\tau} \cdot \mathbf{u_g}$, but, as pointed out by Fofonoff (1981) and Wang and Huang (2004a), this term can only provide energy in an indirect way; what is usually thought of as the work done on the interior circulation is actually work done on the Ekman flow.

We discussed the main pathways of energy in a simple barotropic model of the Southern

Ocean, forced by a band of stochastically varying winds. In our basic experiment, the energy input by the wind stress through s_b is used to push the Ekman drift against the pressure field (p_s). The energy is subsequently stored in potential form via m_s. This reservoir of potential energy can then be tapped (m_b) and used by the pressure field to perform work on the interior flow (p_b). Frictional processes ultimately remove the energy from the system.

It was found that enhanced levels of energy at high frequencies (>0.14 cpd) in the forcing may affect the energetics of the interior flow considerably. Despite the fact that the wind work on the barotropic flow did not change, the time-mean kinetic energy of the interior flow increased by a factor 2.4 when reducing the spectral slope of the forcing from $\gamma = 2.0$ to 0.5. The reason for this is the fact that dissipation is less efficient in removing kinetic energy when a substantial barotropic flow counteracts the Ekman transport in the surface layer. The resulting surplus of energy can then be used by the pressure field to enhance the interior flow.

The mechanisms observed in this model may not control all aspects of the ocean response to wind forcing in a fully stratified ocean. However, the fact that the barotropic response to wind forcing is sensitive to the spectral slope of the wind stress implies that high-frequency winds with realistic spectral slopes are needed to force ocean models, in order to have realistic energetics at high-frequencies.

Acknowledgments. This research was supported by the NASA Ocean Vector Wind Science Team, JPL contract 1222984. The comments of two anonymous reviewers are gratefully acknowledged.

APPENDIX

Having divided the flow into surface and barotropic components, we can represent the sea level fluctuations in terms of the divergences of the respective flow components. Hence we can introduce:

$$\eta_s = -\int_0^t \nabla \cdot \mathbf{U_s} dt'; \eta_b = -\int_0^t \nabla \cdot \mathbf{U_b} dt'. \tag{A1}$$

Here $\mathbf{U_s} = H_m \mathbf{u_s}$ and $\mathbf{U_b} = H\mathbf{u_b}$. Recall that we apply only a zonally-constant zonal wind stress that can be expressed in terms of a spatial pattern $T(y)$, an amplitude τ_0 and a stochastic time series $\sigma(t)$, as introduced before. Suppose that the (meridional) Ekman transport is in balance with the (zonal) wind stress, so that $V_s = -\tau^x/\rho_0 f$. Then we have for η_s:

$$\eta_s = -\int_0^t V_{s,y} dt' = \frac{1}{\rho_0}\int_0^t \left(\frac{\tau^x}{f}\right)_y dt' = \frac{\tau_0}{\rho_0}\left(\frac{T}{f}\right)_y \int_0^t \sigma(t') dt'. \tag{A2}$$

The meridional component of the energy flux g_s then contains the term $\rho_0 g \eta_s V_s$, which can be written as:

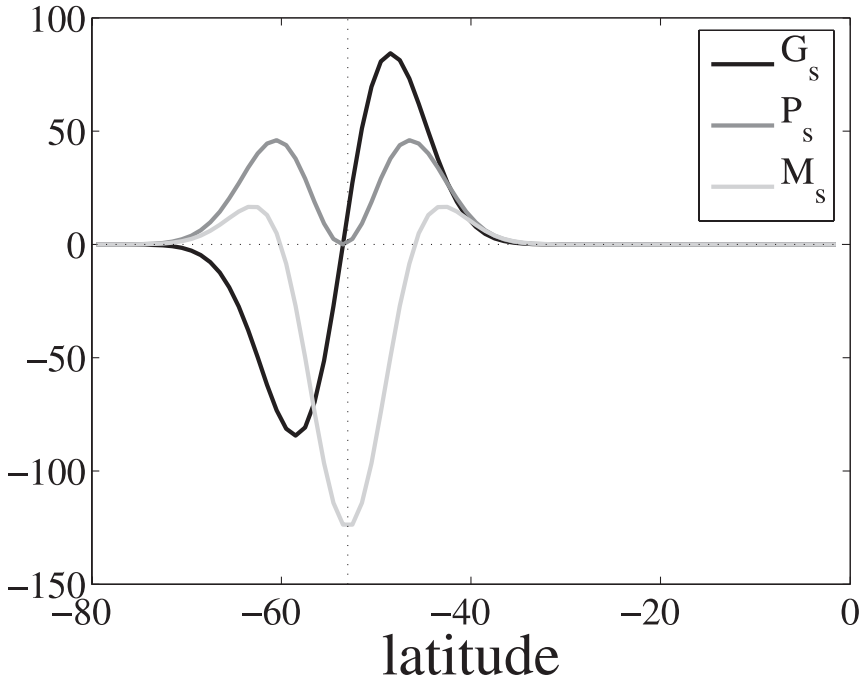

Figure 10. Meridional profiles of $G_{s,s}$ (black line), $P_{s,s}$ (dark gray) and $M_{s,s}$ (light gray). Profile of $G_{s,s}$ is scaled with a factor of $2 \cdot 10^{-6}$.

$$g_{s,s} = \rho_0 g \eta_s V_s = -\frac{g\tau_0^2}{2\rho_0}\left[\left(\frac{T}{f}\right)^2\right]_y \sigma \int_0^t \sigma dt'. \tag{A3}$$

The time-integral of this transport is positive, since:

$$\zeta \equiv \int_0^t \left[\sigma \int \sigma dt''\right] dt' = \frac{1}{2}\int_0^t \frac{d}{dt}\left[\left(\int \sigma dt''\right)^2\right] dt' = \frac{1}{2}\left(\int \sigma dt''\right)^2. \tag{A4}$$

This flux transports energy away from the latitude of maximum wind stress (Fig. 10).

The divergence of this flux gives contributions to the divergence term m_s and the pressure work p_s:

$$m_{s,s} = -\rho_0 g \eta_s V_{s,y} = \frac{g\tau_0^2}{\rho_0}\left[\left(\frac{T}{f}\right)_y\right]^2 \sigma \int_0^t \sigma dt' \tag{A5}$$

describes the potential energy change due to Ekman pumping. It is almost zero at the axis of maximum wind stress, ϕ_τ (Fig. 10), but displays maxima at the latitudes where the meridional gradient of the wind stress is strongest (60S and 46S). Of course, divergences of

the Ekman transport will be largely compensated by convergences of the subsurface flow, but they do not completely erase the signature of the $m_{s,s}$ term.

The term:

$$p_{s,s} = -\rho_0 g V_s \eta_{s,y} = \frac{g\tau_0^2}{\rho_0}\frac{T}{f}\left(\frac{T'}{f}\right)_{yy}\sigma\int_0^t \sigma dt' \tag{A6}$$

measures the work done on the Ekman transport, due to pressure fluctuations induced by divergences of this transport. As shown by Fig. 10, this term is largely negative, meaning that the wind pushes the Ekman transport up-gradient.

REFERENCES

Alford, M. H. 2003. Improved global maps and 54-year history of wind-work on ocean inertial motions. Geophys. Res. Lett., *30,* 1424, doi:10.1029/2002GL016614.

Arbic, B. K., S. T. Garner, R. W. Hallberg and H. L. Simmons. 2004. The accuracy of surface elevations in forward global barotropic and baroclinic tide models. Deep-Sea Res. II, *51,* 3069–3101.

Bell, T. H. 1975. Lee waves in stratified flows with simple harmonic time dependence. J. Fluid Mech., *67,* 705–722.

Chelton, D. B., R. A. DeSzoeke, M. G. Schlax, K. El Naggar and N. Siwertz. 1998. Geographical variability of the first baroclinic Rossby radius of deformation. J. Phys. Oceanogr., *28,* 433–460.

D'Asaro, E. A. 1985. The energy flux from the wind to near-inertial motions in the surface mixed layer. J. Phys. Oceanogr., *15,* 1043–1059.

Dukowicz, J. K. and R. D. Smith. 1994. Implicit free-surface method for the Bryan-Cox-Semtner ocean model. J. Geophys. Res., *99,* 7991–8014.

Fofonoff, N. P. 1981. The Gulf Stream, *in* Evolution of Physical Oceanography: Scientific Surveys in Honor of Henry Stommel, B. A. Warren and C. Wunsch, eds., MIT Press, Cambridge, MA, 112–139.

Frankignoul, C. and P. Müller. 1979. Quasi-geostrophic response of an infinite β-plane ocean to stochastic forcing by the atmosphere. J. Phys. Oceanogr., *9,* 104–127.

Fu, L.-L. 1981. Observations and models of inertial waves in the deep ocean. Rev. Geophys. Space Phys., *19,* 141–170.

Garrett, C. and W. Munk. 1979. Internal waves in the ocean. Ann. Rev. Fluid Mech., *11,* 339–369.

Gill, A. E. 1982. Atmosphere-Ocean Dynamics, Academic Press, NY, 662 pp.

Gill, A. E., J. S. A. Green and A. J. Simmons. 1974. Energy partition in the large-scale ocean circulation and the production of mid-ocean eddies. Deep-Sea Res., *21,* 499–528.

Gille, S. T. 2005. Statistical characterization of zonal and meridional ocean wind stress. J. Atmos. Ocean. Tech., *22,* 1353–1372.

Ginis, I. and G. Sutyrin. 1995. Hurricane-generated depth-averaged currents and sea surface elevation. J. Phys. Oceanogr., *25,* 1218–1242.

Hirose, N., I. Fukumori and V. Zlotnicki. 2001. Modeling the high-frequency barotropic response of the ocean to atmospheric disturbances: Sensitivity to forcing, topography, and friction. J. Geophys. Res., *106,* 30987–30995.

Holland, W. R. 1975. Energetics of baroclinic oceans, *in* Numerical Models of the Ocean Circulation, *5*, National Academy of Sciences, Washington, DC, 168–177.

Huang, R. X. 1998. Mixing and available potential energy in a Boussinesq ocean. J. Phys. Oceanogr., *28,* 669–678.

Ivchenko, V. O., A. M. Treguier and S. E. Best. 1997. A kinetic energy budget and internal instabilities in the Fine Resolution Antarctic Model. J. Phys. Oceanogr., *27,* 5–22.

Jayne, S. R. and L. C. St. Laurent. 2001. Parameterizing tidal dissipation over rough topography. Geophys. Res. Lett., *28,* 811–814.

Koblinsky, C. J. 1990. The global distribution of *f*/*H* and the barotropic response of the ocean. J. Geophys. Res., *95,* 3213–3218.

Large, W. G., W. R. Holland and J. C. Evans. 1991. Quasi-geostrophic ocean response to real wind forcing: the effects of temporal smoothing. J. Phys. Oceanogr., *21,* 998–1017.

MacCready, P., G. Pawlak, K. A. Edwards and R. McCabe. 2001. Form drag on ocean flows, *in* Near Boundary Processes and Their Parameterization: Proc. 'Aha Huliko'a Hawaiian Winter Workshop, University of Hawaii at Monoa, Honolulu, HI, 119–130.

Marshall, J., A. Adcroft, C. Hill, L. Perelman and C. Heisey. 1997a. A finite-volume, incompressible Navier-Stokes model for studies of the ocean on parallel computers. J. Geophys. Res., *102,* 5753–5766.

Marshall, J., C. Hill, L. Perelman and A. Adcroft. 1997b. Hydrostatic, quasi-hydrostatic, and non-hydrostatic ocean modelling. J. Geophys. Res., *102,* 5733–5752.

McWilliams, J. C., W. R. Holland and J. H. S. Chow. 1978. A description of numerical Antarctic Circumpolar Currents. Dyn. Atmos. Oceans, *2,* 213–291.

Müller, P. and C. Frankignoul. 1981. Direct atmospheric forcing of geostrophic eddies. J. Phys. Oceanogr., *11,* 287–308.

Munk, W. and C. Wunsch. 1998. Abyssal recipes II: energetics of tidal and wind mixing. Deep-Sea Res. I, *45,* 1977–2010.

Nowlin, W. D. and J. M. Klinck. 1986. The physics of the Antarctic Circumpolar Current. Rev. Geophys., *24,* 469–491.

Oort, A. H., L. A. Anderson and J. P. Peixoto. 1994. Estimates of the energy cycle of the oceans. J. Geophys. Res., *99,* 7665–7688.

Pedlosky, J. 1987. Geophysical Fluid Dynamics, Springer-Verlag, NY, 710 pp.

Peterson, R. G. 1988. On the transport of the Antarctic Circumpolar Current through Drake Passage and its relation to wind. J. Geophys. Res., *93,* 13993–14004.

Pollard, R. T. and R. C. Millard. 1970. Comparison between observed and simulated wind-generated inertial oscillations. Deep-Sea Res., *17,* 813–821.

Scott, R. B. 1999. Mechanical energy flux to the surface geostrophic flow using TOPEX/Poseidon data. Phys. Chem. Earth (A), *24,* 399–402.

Shay, L. K., S. W. Chang and R. L. Elsberry. 1990. Free surface effects on the near-inertial ocean current response to a hurricane. J. Phys. Oceanogr., *20,* 1405–1424.

Simmons, H. L., R. W. Hallberg and B. K. Arbic. 2004. Internal wave generation in a global baroclinic tide model. Deep-Sea Res. II, *51,* 3043–3068.

Stammer, D., C. Böning and C. Dieterich. 2001. The role of variable wind forcing in generating eddy energy in the North Atlantic. Prog. Oceanogr., *48,* 289–311.

Thompson, D. W. J. and J. M. Wallace. 2000. Annular modes in the extratropical circulation. Part I: Month-to-month variability. J. Clim., *13,* 1000–1016.

Veronis, G. 1956. Partition of energy between geostrophic and non-geostrophic ocean motions. Deep-Sea Res., *3,* 157–177.

Veronis, G. and H. Stommel. 1956. The action of variable wind stresses on a stratified ocean. J. Mar. Res., *15,* 43–75.

Wang, W. and R. X. Huang. 2004a. Wind energy input to the Ekman layer. J. Phys. Oceanogr., *34,* 1267–1275.

——2004b. Wind energy input to the surface waves. J. Phys. Oceanogr., *34,* 1276–1280.

Watanabe, M. and T. Hibiya. 2002. Global estimates of the wind-induced energy flux to inertial motions in the surface mixed layer. Geophys. Res. Lett., *29,* doi:10.1029/2001GL014422.

Weijer, W. 2005. High-frequency wind forcing of a channel model of the ACC: Normal mode excitation. Ocean Model., *9,* 31–50.

Weijer, W. and S. T. Gille. 2005. Adjustment of the Southern Ocean to wind forcing on synoptic time scales. J. Phys. Oceanogr., *35,* 2076–2089.

Willebrand, J., S. G. H. Philander and R. C. Pacanowski. 1980. The oceanic response to large-scale atmospheric disturbances. J. Phys. Oceanogr., *10,* 411–429.

Wunsch, C. 1998. The work done by the wind on the oceanic general circulation. J. Phys. Oceanogr., *28,* 2332–2340.

Wunsch, C. and R. Ferrari. 2004. Vertical mixing, energy, and the general circulation of the oceans. Ann. Rev. Fluid Mech., *36,* 281–314.

Received: *2 March, 2005;* revised: *19 July, 2005.*